Future climate change scenarios shaped by inter-model differences in Atlantic Meridional Overturning Circulation response

Katinka Bellomo[1], Michela Angeloni[2], Susanna Corti[3], and Jost von Hardenberg[4]

[1]Institute of Atmospheric Sciences and Climate, National Research Council, Turin, Italy
[2]Department of Physics and Astronomy, University of Bologna, Bologna, Italy
[3]Institute of Atmospheric Sciences and Climate, National Research Council, Bologna, Italy
[4]Politecnico di Torino, Turin, Italy

November 30, 2022

Abstract

In climate model simulations of future climate change, the Atlantic Meridional Overturning Circulation (AMOC) is projected to decline. However, the impacts of this decline, relative to other changes, remain to be identified. Here we address this problem by analyzing 30 idealized abrupt-4xCO2 climate model simulations. We find that in models with larger AMOC decline, there is minimum warming in the North Atlantic, a southward displacement of the Inter-tropical Convergence Zone (ITCZ) and a poleward shift of the mid-latitude jet. The changes in the models with smaller AMOC decline are drastically different: there is a relatively larger warming in the North Atlantic, the precipitation response exhibits a wet-get-wetter, dry-get-drier pattern, and there are smaller displacements of the mid-latitude jet. Our study indicates that the AMOC is a major source of inter-model uncertainty, and continued observational efforts are needed to constrain the AMOC response in future climate change.

FRONT MATTER

Title

- Full Title: "**Future climate change scenarios shaped by inter-model differences in Atlantic Meridional Overturning Circulation response**"
- Short Title: "**Uncertainty in future climate change driven by ocean circulation response**"

Authors

Katinka Bellomo[1*], Michela Angeloni[2,1], Susanna Corti[3], Jost Von Hardenberg[4,1]

Affiliations

[1] Institute of Atmospheric Sciences and Climate, National Research Council (ISAC-CNR), Turin, Italy

[2] Department of Physics and Astronomy, University of Bologna, Bologna, Italy

[3] Institute of Atmospheric Sciences and Climate, National Research Council (ISAC-CNR), Bologna, Italy

[4] Department of Environment, Land and Infrastructure Engineering, Politecnico di Torino, Turin, Italy

* corresponding author: k.bellomo@isac.cnr.it

Abstract

In climate model simulations of future climate change, the Atlantic Meridional Overturning Circulation (AMOC) is projected to decline. However, the impacts of this decline, relative to other changes, remain to be identified. Here we address this problem by analyzing 30 idealized abrupt-4xCO2 climate model simulations. We find that in models with larger AMOC decline, there is a minimum warming in the North Atlantic, a southward displacement of the Inter-tropical Convergence Zone (ITCZ) and a poleward shift of the mid-latitude jet. The changes in the models with smaller AMOC decline are drastically different: there is a relatively larger warming in the North Atlantic, the precipitation response exhibits a wet-get-wetter, dry-get-drier pattern, and there are smaller displacements of the mid-latitude jet. Our study indicates that the AMOC is a major source of inter-model uncertainty, and continued observational efforts are needed to constrain the AMOC response in future climate change.

MAIN TEXT

Introduction

The Atlantic Meridional Overturning Circulation (AMOC) plays a crucial role in the climate system by regulating the global transport of heat, carbon and freshwater. It is estimated that annually as much as ~0.5 PW of heat is carried across the equator into the North Atlantic solely by the AMOC, which is responsible for making the entire northern hemisphere ~1°C warmer than the southern hemisphere (Talley 2008, Buckley and Marshall 2016, Weijer et al. 2020a). This inter-hemispheric asymmetry in surface temperature largely contributes to shift the Inter-tropical Convergence Zone (ITCZ), where tropical precipitation is heaviest, north of the equator at about 5°N, thus influencing global rainfall and atmospheric circulation patterns (Frierson et al. 2013, Marshall et al. 2014).

In addition, the AMOC has been identified as one of the tipping elements in the climate system (Lenton et al. 2013). In fact, abrupt changes in the AMOC have been implicated in glacial-interglacial transitions (Broecker 1997, Rahmstorf 2002, Broecker 2003), such as Dansgaard-Oeschger oscillations (Dansgaard et al. 1993). The role of the AMOC in amplifying these transitions is supported by deep-ocean proxy data (Burckel et al. 2015, Henry et al. 2016). The potential impacts of an abrupt AMOC shutdown have been examined in idealized climate model simulations in which the AMOC is artificially halted. These simulations are often referred to as 'water hosing' experiments, and show that an AMOC shutdown would cause a widespread cooling of the northern hemisphere by several degrees, increased sea ice in the North Atlantic and a southward shift of the ITCZ (Zhang and Delworth 2005, Vellinga and Wood 2008, Jackson et al. 2015). Even a smaller decline would have widespread impacts (Zhang et al. 2019, Liu et al. 2020).

Since there is increasing evidence that the AMOC has slowed over the last century (Rahmstorf et al. 2015, Ceasar et al. 2018), direct observations of the AMOC started in 2004 with the RAPID-MOCHA array project to monitor the stability of the AMOC (McCarthy et al. 2012, Weijer et al. 2020a). Also these observations show a downward trend (Robson et al. 2013, Smeed et al. 2014, Smeed et al. 2018), although internal variability is large (Zhao and Johns 2014, Jackson et al. 2016, Frajka-Williams et al. 2019). While it is not yet possible from observations to quantify the anthropogenic contribution to this decline, model projections of future climate change show a further decline of the AMOC into the 21st century in response to greenhouse gas forcing (Collins et al. 2013, Weijer et al. 2020). The further decline has been ascribed to a decrease in the density of sea water in the Sub-Polar North Atlantic (SPNA) (Sevellec et al. 2017, Liu et al. 2019, Levang and Schmitt 2020). A direct consequence of the AMOC weakening is a reduced warming in the SPNA Sea Surface Temperature (SST), often referred to as the 'North Atlantic Warming Hole' (NAWH)

(Drijfhout et al. 2012, Winton et al. 2013, Marshall et al. 2015, Ceasar et al. 2018, Gervais et al. 2018, Liu et al. 2020, Keil et al. 2020). The NAWH, by changing the baroclinicity of the atmosphere, could affect the large-scale atmospheric response to global warming (Gervais et al. 2019); however, the precise impacts are unknown since there is large inter-model spread in the projections of the NAWH anomaly and its spatial extent (Menary and Wood 2017).

Although the AMOC in current climate models may be too stable (Liu et al. 2017, Weijer et al. 2020a), an AMOC shutdown within the next century is deemed unlikely (Collins et al. 2013). However, there is a wide range in the projected decline rates (Gregory et al. 2005, Cheng et al. 2013, Kostov et al. 2014, Weijer et al. 2020), and the consequences of the inter-model spread in the AMOC response remain uncertain. In order to narrow down the inter-model range in projections of future climate change, it is crucial to identify the sources of uncertainty and their impacts. Hence, it is of primary interest to describe and quantify the global impacts caused by the inter-model spread in the AMOC response. In this study, we investigate this issue by examining an ensemble of 30 abrupt-4xCO2 simulations from the Coupled Model Intercomparison Project phase 5 ('CMIP5', Taylor et al. 2012) and phase 6 ('CMIP6', Eyring et al. 2016).

Results

Inter-model spread in the AMOC response

The AMOC strength anomalies at 26.5°N in the abrupt-4xCO2 experiments are shown for the 12 CMIP5 models in fig. 1a and the 18 CMIP6 models in fig. 1b. All models show a decline from the pre-industrial control climate, but the inter-model range is larger in the newer generation of models (fig. 1b). In CMIP6, there are also more models that exhibit a stronger AMOC decline. The AMOC decline in CMIP5 ranges between about -4 Sv and -10 Sv (-27% to -58%) while in CMIP6 between about -1.5 Sv and -17.5 Sv (-18% to -74%). Even if the decline is larger in the newer models, none of them show an abrupt shutdown of the AMOC (the lowest value is 5.50 Sv), although a collapse of the AMOC may be an overlooked possibility in state-of-the-art climate models (Liu et al. 2017). On the contrary, we note that in some models the AMOC starts to recover towards the end of the abrupt-4xCO2 simulation. For reference, Table S1 reports the mean AMOC strength computed from the pre-industrial control experiments, the AMOC index change, and other statistics.

To further investigate the differences in the AMOC decline across the models, we divide the CMIP5+CMIP6 ensemble in two groups: the average of the 10 models with the largest AMOC declines is referred to as the 'large AMOC decline' group, while the average of the 10 models with the smallest AMOC declines is referred to as the 'small AMOC decline' group (Table S2). For each of these groups, we calculate the change in the abrupt-4xCO2 simulations from the pre-industrial control mean climate (see Materials and Methods). Table 1 shows that differences between the mean values of AMOC diagnostics are statistically different between the two groups. Fig. 1c and 1d show the changes in the North Atlantic transects of the meridional overturning stream-function in the two groups. The decrease in the AMOC tends to be more pronounced between 25°N and 40°N in both groups. We note that models with stronger AMOC in the mean climate (contours in fig. 1c and 1d) generally belong to the large AMOC decline group, while models with weaker AMOC in the mean climate belong to the small AMOC decline group (fig. S1), which is consistent with previous findings (Gregory et al. 2005).

While an inter-model spread in the AMOC response to climate change has been recognized before (Chang et al. 2013, Collins et al. 2013, Weijer et al. 2020b), here we investigate whether this spread leads to significant differences in global climate impacts. In order to separate the effect of the AMOC response from other processes, in addition to dividing models into large and small AMOC decline responses, in the following we also divide each model by its respective change in Global Mean Temperature (ΔGMT), defined as global mean near surface air temperature change. This reduces the influence of the inter-model spread due to other feedback processes (see Materials and Methods), and shows the expected change for each 1°C of global warming, thus facilitating comparisons with other climate change scenarios. We note that ΔGMT itself is weakly dependent on ΔAMOC (fig. S2); however, since the spread is large and the Pearson's r correlation coefficient between ΔGMT and ΔAMOC is only 0.31, we argue that other climate feedbacks are more important in determining ΔGMT (Collins et al. 2013, Zelinka et al. 2020, Lin et al. 2019).

Surface temperature change

The surface temperature change is shown in fig. 2 for the large AMOC decline group (fig. 2a) and small AMOC decline group (fig. 2b). Fig. 2a and 2b are the changes from the pre-industrial control experiment, while fig. 2c is their difference (large minus small AMOC change). The surface temperature at each grid point represents the local temperature change per degree of global warming. Over the ocean, the surface temperature is the Sea Surface Temperature (SST). We interpret fig. 2c as the expected impact of a larger AMOC decline in a future climate change scenario, compared to a smaller AMOC decline. In fig. 2c, stippling indicates where the differences in the simulated climate change between the small and large AMOC groups are statistically significant.

Fig. 2a shows that in the models with the largest AMOC declines, there is a minimum SST warming in the North Atlantic. This minimum warming has been associated with the decline of the AMOC in earlier climate change studies, and is often referred to as the North Atlantic Warming

Hole (NAWH). On the other hand, fig. 2b (small AMOC decline) shows no NAWH, but actually a relatively large SST change in the sub-polar North Atlantic (SPNA). Fig. 2c confirms that the change in surface temperature is drastically different between the two groups, especially in the North Atlantic and the Arctic, but also in the Southern Ocean in the areas of deep-water formation. In addition, the difference in absolute near surface air temperature change between the large and small AMOC decline groups (fig. S3), which is not divided by ΔGMT, is strikingly similar to the response to a disruption of the AMOC in water hosing model experiments (Zhang and Delworth 2005, Jackson et al. 2015, Vellinga and Wood 2008, Woollings et al. 2012). The similarity between these earlier experiments and our results further supports the hypothesis that the differences in the patterns of surface temperature change shown in fig. 2 are largely influenced by the difference in AMOC decline between the large and the small AMOC groups, rather than by other processes. If instead of choosing the top and bottom 10 models based on AMOC decline, we simply divide the models in half based on the median AMOC decline, we still obtain the same temperature change pattern, although the absolute difference in each grid point is smaller, and there is overall less statistical significance. We also obtain similar results if we repeat this analysis only in the CMIP5 (or CMIP6) archive (not shown).

Fig. 2d shows the SPNA SST change (area average of 50°N-70°N SST over the North Atlantic Ocean) divided by ΔGMT, against the respective AMOC change for each of the 30 models in the CMIP5+CMIP6 ensemble. This scatterplot shows that the relationship between the SPNA SST change and AMOC change is robust across all models, and linear: the larger the AMOC decline, the smaller the projected temperature increase in the SPNA, and vice versa. The R^2 of the least-square linear regression is 0.63, while the Pearson's r correlation coefficient is 0.8. We interpret this relationship as the consequence of a greater reduction in ocean heat transport in the North Atlantic as the decline in AMOC strength becomes larger, which acts to slow down the temperature increase. The slower AMOC also effectively reduces Arctic amplification in the large AMOC decline group (fig. S4). Further, fig. 2d shows that the influence of AMOC on surface temperature is not limited to the models with the largest and smallest AMOC declines, but applies to all models. In fact, the key finding here is that the inter-model spread in the AMOC response is a major driver of uncertainty in SPNA SST change.

In summary, the AMOC decline acts as a regional negative feedback, but only in the models featuring a large AMOC decline (c.f. fig. 2a with 2b). This means that, based on whether the AMOC decline is large or small, there are drastically different changes in North Atlantic SST in the models. Table 1 further shows that the differences of the means of SPNA SST change and ΔGMT between the two groups are statistically significant. We now investigate whether the inter-model spread in the AMOC response, through its influence on SST, may affect other aspects of climate change, including precipitation and large-scale atmospheric circulation.

Precipitation change

Fig. 3 shows precipitation change divided by ΔGMT (units of mm/day/°C) in the large AMOC decline group (fig. 3a), small AMOC decline group (fig. 3b), and their difference (fig. 3c). In fig. 3a, 3b and 3c, superimposed in contours is the ensemble mean of the precipitation climatology computed from all 30 CMIP5+CMIP6 models. As for fig. 2, fig. 3a and fig. 3b show the changes between the abrupt-4xCO2 simulations and the pre-industrial control. In fig. 3c, stippling indicates where the differences in the simulated climate change between the small and large AMOC groups are statistically significant.

Fig. 3a shows interesting dissimilarities from 3b, which we attribute to the amplitude of AMOC decline driving different patterns of surface temperature change. Generally speaking, the small AMOC group features the precipitation changes that we expect from the wet-get-wetter/dry-get-drier paradigm (Held and Soden 2006), according to which precipitation over the ocean will increase in wet regions and will decrease over dry regions. In contrast, the large AMOC group deviates from this paradigm. For example, over the North Atlantic mid-latitudes, precipitation is projected to decrease over the Gulf Stream and over the SPNA in the large AMOC group (fig. 3a), in stark contrast to the small AMOC group where the precipitation anomaly is of opposite sign and is actually projected to increase over those regions (fig. 3b). A reduced rainfall over the SPNA is expected from an abrupt decline in the AMOC, and has been explained by a reduced evaporation from the ocean and a decrease in eddy moisture transport (Liu et al. 2020, Sun et al. 2018, Hand et al. 2019). These same mechanisms may operate in response to 4xCO2, but only in the models featuring a large AMOC decline. In the Pacific Ocean, in the large AMOC decline group, there seems to be a more pronounced El Niño like response, with precipitation increasing in the eastern side of the equatorial Pacific and decreasing in the western side. This is associated with a larger warming in SST in the eastern side in the large AMOC decline group than in the small AMOC decline group (fig. 2c). While this difference has poor statistical significance, a negative correlation in which negative SST anomalies associated with the Atlantic Multidecadal Variability are linked with positive SST anomalies in the eastern equatorial Pacific (and vice versa), has been noted before (Levine et al. 2018), and is consistent with our results.

Focusing on the Atlantic sector, in fig. 3d we compute the zonal mean precipitation change in the large AMOC group (blue) and small AMOC group (red). Statistical significance is indicated by the round markers on the blue and red lines. For reference, the zonal mean precipitation climatology computed from all 30 CMIP5+CMIP6 models is plotted in green. Some inter-model spread exists, but the differences between the groups are clear here: while, compared to the climatology (green), the small AMOC decline group (red) exhibits the expected wet-get-wetter and dry-get-drier behavior with increase in precipitation at the equator, decrease in the subtropics, and increase in the northern hemisphere mid-latitudes, the large AMOC decline group shows a completely different response. In the large AMOC decline group, the peak of precipitation in the tropics (ITCZ), which normally sits above the equator in the northern hemisphere in the annual mean (green), locally decreases and the anomaly shifts to the southern hemisphere. The shift of the ITCZ is forced by the larger equator to pole gradient in temperature change, and reduced Arctic amplification, in the large AMOC decline group (fig. S4). In the mid-latitudes, where the precipitation change is positive in the small AMOC decline group, it is of opposite sign in the large AMOC decline group (fig. 3d).

The Indian monsoon is also affected. While in both groups precipitation increases (fig. 3a and fig. 3b) especially in JJA (not shown), in the large AMOC decline group precipitation does not increase as much as in the small AMOC group (fig. 3c). This suggests that the AMOC may modulate the response of the Indian monsoon to climate change, with important societal implications. A connection between the AMOC, the warming of the Indian Ocean and the summer monsoon has been noted before both in climate change scenarios (Hu and Fedorov 2019) and inter-decadal variability (Goswami et al. 2006), and has been associated with the north-south temperature gradient across Eurasia.

Atmospheric circulation change

Given that the NAWH influences the north-south gradient in surface temperature (fig. S4), which may affect the mid-latitude jet, we now investigate whether there are any significant differences in the response of the mid-latitude easterly winds in relation to the AMOC decline. Fig. 4 shows the zonal mean easterly wind change in the abrupt-4xCO2 simulations from the pre-industrial control mean in boreal winter (DJF) for the large AMOC decline group (fig. 4a), small AMOC decline group (fig. 4b), and their difference (fig. 4c). Each model is divided by ΔGMT (units of m/s/°C). The difference shown in fig. 4c, similarly to the other figures, is attributed to the AMOC response difference between the two groups. Superimposed in contours in fig. 4a, 4b and 4c is the climatological mean, while stippling in fig. 4c indicates statistical significance.

The patterns of change are similar in the large and small AMOC groups, however their difference (fig. 4c) reveals that in the northern hemisphere there is a statistically significant increase in wind speed poleward of the climatological maximum, and a decrease to the south. In the southern hemisphere, changes are similar during austral winter (JJA) (not shown). From a purely thermodynamic standpoint, in response to climate change there is a tug of war between the contrasting effects on the jet of Arctic amplification and tropical upper troposphere heating (Oudar et al. 2020, Woollings et al. 2012, Chen et al. 2020). While Arctic amplification would, on its own, push the mid-latitude jet closer to the equator, the tropical heating together with the expansion of the Hadley cell would push the jet poleward. Fig. 4c shows that the effect of the tropical heating is stronger when there is a large AMOC decline because Arctic amplification is reduced (fig. S4).

Further examination reveals that this mechanism explains the changes in the thermally driven upper-level jet, but not the low-level eddy driven jet. Fig. 4d shows the change in the latitude of the maximum easterly wind speed at 250hPa divided by ΔGMT against the AMOC change for each model. There is a linear relation between the amplitude of the AMOC decline and the northward displacement of the jet: the stronger the AMOC decline, the more the jet is displaced poleward. In contrast, in models where the AMOC decline is smaller, there is actually an equatorward displacement. When we exclude the two outliers (SAM0-UNICON and GISS-E2-1-G), the R^2 of the least-square regression line in fig. 4d is 0.48, while the Pearson's r correlation coefficient is -0.7. We do not find a similarly robust relationship between the eddy driven jet at 850hPa and AMOC change, which could be explained by the fact that the NAWH has been found to have a relatively weak impact on the eddy driven jet, compared to other drivers (Oudar et al. 2020).

Discussion

While the AMOC is expected to decline in response to increasing greenhouse gases, the role of the AMOC decline in future climate change is unclear. In this study, we address this question specifically examining how the inter-model range in the AMOC response affects projected climate change in a suite of climate models participating in the CMIP5 and CMIP6 archives.

We find that in models with larger AMOC decline, the reduced northward heat transport by ocean circulation acts as a negative feedback on SST warming in the North Atlantic; however, in models with smaller AMOC decline, this effect is absent and there is actually a relatively larger warming in the SPNA. We find that these drastically different SST scenarios, caused by the inter-model spread in the AMOC decline, are associated with large-scale impacts on precipitation and mid-latitude circulation responses. In the models with larger AMOC decline, the precipitation over the oceans does not follow the canonical wet-get-wetter/dry-get-drier paradigm, but there is a southward shift in the ITCZ and a reduction in precipitation over the Gulf Stream and the SPNA. In addition, the mid-latitude thermally driven jet tends to move poleward. In contrast, in the models with smaller AMOC decline, the precipitation response is as expected by the wet-get-wetter/dry-get-drier paradigm, while the jet's displacement is either small or equatorward. The differences in the response of large-scale atmospheric circulation and precipitation are also partly explained by the reduction in Arctic amplification caused by a larger AMOC decline.

Our results are in agreement with, and extend, the findings of a recent study (Liu et al. 2020), which was based on idealized model experiments with one global climate model. We also find that the differences between the large AMOC group and small AMOC group, which we interpret as driven by the AMOC response, are remarkably similar to the climate change patterns expected by a shut-down of the AMOC, which has been largely investigated in water hosing simulations but in the absence of increasing greenhouse gases (Zhang and Delworth 2005, Winton et al. 2013, Jackson et al. 2015). One interesting result is that a decline in the AMOC has a cooling effect on Europe, but not on North America (fig. 2c and fig. S3c), which partly contradicts a previous study arguing that the effect of the AMOC on surface temperature is zonally uniform in the northern hemisphere (Seager et al. 2002). The main limitation of our study is that it remains difficult to fully separate the influence of the AMOC from other processes using the existing experiments in the CMIP5 and CMIP6 archives. Future work should focus on refining a method to better isolate the AMOC from other feedback mechanisms.

In conclusion, the key finding of this work is that the inter-model spread in the AMOC response drives different climate change scenarios in a number of societally important atmospheric variables. The implication is that there is much uncertainty arising solely from the inter-model spread in the AMOC response. We have found a small dependence of the amplitude of the AMOC decline on the mean strength of the AMOC, which confirms previous findings (Gregory et al. 2005). In addition, there has been recent progress in showing that model biases in the simulation of the mean climate are connected to the amplitude of the AMOC response (Hu et al. 2020). This suggests that continued observational efforts in the North Atlantic can help constrain the simulation of the mean climate, thereby reducing the uncertainty in projections of future climate change.

Materials and Methods

Data

In this study, we examine the pre-industrial control and abrupt-4xCO2 experiments from the CMIP5 and CMIP6 archives. In the pre-industrial control experiment, the atmospheric concentration of CO2 is held fixed at 280ppm and the model variability is entirely driven by internal processes. In the abrupt-4xCO2 experiment the concentration of CO2 is suddenly increased to 4 times the value of the pre-industrial control experiment (1120 ppm) and held at this value throughout the experiment. We use the model output of 12 CMIP5 and 18 CMIP6 models. Table S1 lists the models used in this study, and shows relevant statistics.

Methods

All datasets are interpolated to a common 2.5×2.5 grid before the analysis. We use only one ensemble member for each model (r1i1p1 for CMIP5 and r1i1p1f1 for CMIP6), and we find no significant differences when additional ensemble members are included for models that made them available. For the EC-Earth3 model, the r1i1p1f1 ensemble member was not available, hence we use r3i1p1f1.

We calculate the AMOC index as the maximum of the ocean meridional overturning stream-function at 26.5 °N in the Atlantic Ocean for each year (results are similar using 40°N). We note that for the model FGOALS-f3-L we were unable to access the ocean meridional stream-function from the pre-industrial control, hence for this model we use the first year of the abrupt-4xCO2 simulation to compute the mean AMOC strength. This choice is motivated by the fact that for all the other models there is a very good agreement between the value of the AMOC strength computed from the first year of the abrupt-4xCO2 simulation and the mean of the pre-industrial control (fig. S5). The Pearson's r correlation coefficient is 0.98.

To quantify the influence of the inter-model spread in the AMOC response, we first calculate the impact of the quadrupling of CO2 as the difference between the mean of the years 90 through 139 (total of 150 years) in the abrupt-4xCO2 simulation and the mean of the years 50 through 199 (total of 250 years) in the pre-industrial control simulation for each variable and all models. Choosing other time frames from the pre-industrial control to compute the differences leads to similar results. We decided to use the years 90 to 139 for the abrupt-4xCO2 simulations because after year 90 all of the models reach a plateau in the AMOC response (fig. 1). We use the year 139 as the final year because we want to maximize the number of models available to analyze, and one of the models only provides 140 years instead of 150. Moreover, some models show a recovery of the AMOC towards the end of the abrupt-4xCO2 simulation (fig. 1), thus excluding the last 10 years limits this influence.

To specifically investigate the role of the AMOC in driving climate changes relative to other processes, we form 2 groups of models based on the AMOC index change: the 'large AMOC decline' group includes the 10 models with the largest AMOC declines, while the 'small AMOC decline' group includes the 10 models with the smallest AMOC declines (marked as red/blue in Table S2). We interpret the difference between these two groups ('large AMOC decline' minus 'small AMOC decline') as the effect of the AMOC response on the differences in the simulated climate change impacts between the 2 groups. We also divide each model by their respective change in Global Mean Temperature (ΔGMT) to reduce the influence of other processes and feedbacks. ΔGMT is computed as the area averaged global mean near surface air temperature change from the pre-industrial control experiments. If instead of dividing the groups based on the absolute value of AMOC strength in units of Sv, we divide based on the percent AMOC change from the pre-industrial control strength, we find similar results. An alternative method to identify the role of the AMOC is to perform linear regressions of each variable on the AMOC anomalies; however, this approach masks the distinctive patterns (e.g., precipitation in fig. 3) that we want to highlight.

To investigate whether the changes associated with the AMOC response are statistically significant, we perform a two-tailed t-test on the differences between the large and small AMOC decline groups, assuming equal variance in the two groups. Where this test indicates that results are statistically significant at the 90% level, we argue that the differences are driven by the different AMOC responses in the two sets of models. This is indicated by the '*' stippling in the figures. We further assess statistical significance by forming 2 groups of 500 samples of randomly picked 10 models among the 30 CMIP5+CMIP6 models, without repetition. We perform a t-test and a z-test to check whether the difference between large and small AMOC decline groups is statistically different from the 500 differences of the randomly chosen 2 groups. The results of the random tests show even better significance for all variables than the two-tailed t-test, hence they are not shown.

We provide measures of inter-model 'reliability' to assess whether within the large and small AMOC decline groups there is good inter-model agreement. We use two definitions. In fig. 3 and fig. 4, reliability is indicated by the '/' stippling and is the defined where at least 80% of the models in each group agree on the sign of the change from the pre-industrial control climatology. This definition is reasonable when the expected change could be either positive or negative. However for other variables, such as surface temperature, the change in response to $4xCO_2$ forcing is always positive for all the models. For this reason, in fig. 1, 2, S3 and S4, reliability is indicated by the 'x' stippling, which is defined where at least a certain percentage of models in each group agree on the sign of the difference between the model's change and the median change of all CMIP5+CMIP6 models. The specific percent threshold for the 'x' stippling depends on the variable, and is specified in the figure captions.

Supplementary Materials

Fig. S1: Dependence of AMOC change on the mean AMOC strength.
Fig. S2: Dependence of global mean temperature change on AMOC change.
Fig. S3: Near surface air temperature.
Fig. S4: Zonal mean air temperature.

Fig. S5: Estimates of mean AMOC strength.

Table S1: List of CMIP5 and CMIP6 models.

Table S2: Large and small AMOC decline groups.

References

Broecker W. S., 1997: Thermohaline circulation, the Achilles heel of our climate system: Will man-made CO2 upset the current balance?, Science, 278, 5343, 1582–1588, https://doi.org/10.1126/science.278.5343.1582.

Broecker W. S., 2003: Does the trigger for abrupt climate change reside in the ocean or in the atmosphere?, Science, 300, 5625, 1519–1522, https://doi.org/10.1126/science.1083797.

Buckley M. W. and Marshall J., 2016: Observations, inferences, and mechanisms of the Atlantic Meridional Overturning Circulation: A review, Reviews of Geophysics, 54, 5–63, https://doi.org/10.1002/2015RG000493.

Burckel P., Waelbroeck C., Gherardi J. M., Pichat S., Arz H., Lippold J., Dokken T., and Thil F., 2015: Atlantic Ocean circulation changes preceded millennial tropical South America rainfall events during the last glacial, Geophys. Res. Lett., 42, 411– 418, https://doi.org/10.1002/2014GL062512.

Caesar L., Rahmstorf S., Robinson A., Feulner G., and Saba V., 2018: Observed fingerprint of a weakening Atlantic Ocean overturning circulation, Nature 556, 191–196, https://doi.org/10.1038/s41586-018-0006-5.

Chen G., Zhang P., and Lu J., 2020: Sensitivity of the latitude of the westerly jet stream to climate forcing, Geophysical Research Letters, 47, e2019GL086563, https://doi.org/10.1029/2019GL086563.

Cheng W., Chiang J. C. H., and Zhang D., 2013: Atlantic Meridional Overturning Circulation (AMOC) in CMIP5 Models: RCP and Historical Simulations, Journal of Climate, 26, 7187–7197, https://doi.org/10.1175/JCLI-D-12-00496.1.

Collins M., Knutti R., Arblaster J., et al., 2013: Long-term climate change: Projections, commitments and irreversibility. In Climate Change 2013: The Physical Science Basis. Contribution of Working Group I to the Fifth Assessment Report of the Intergovernmental Panel on Climate Change. T.F. Stocker, D. Qin, G.-K. Plattner, M. Tignor, S.K. Allen, J. Doschung, A. Nauels, Y. Xia, V. Bex, and P.M. Midgley, Eds. Cambridge University Press, pp. 1029-1136, https://doi.org/10.1017/CBO9781107415324.024.

Dansgaard W., and Coauthors, 1993: Evidence for general instability of past climate from a 250-kyr ice-core record, Nature, 364, 218–220, https://doi.org/10.1038/364218a0.

Drijfhout S., van Oldenborgh G. J., and Cimatoribus A., 2012: Is a Decline of AMOC Causing the Warming Hole above the North Atlantic in Observed and Modeled Warming Patterns?, Journal of Climate, 25, 8373–8379, https://doi.org/10.1175/JCLI-D-12-00490.1.

Eyring, V., Bony, S., Meehl, G. A., Senior, C. A., Stevens, B., Stouffer, R. J., and Taylor, K. E., 2016: Overview of the Coupled Model Intercomparison Project Phase 6 (CMIP6) experimental design and organization, Geosci. Model Dev., 9, 1937–1958, https://doi.org/10.5194/gmd-9-1937-2016.

Frajka-Williams E., Ansorge I. J., Baehr J., et al., 2019: Atlantic Meridional Overturning Circulation: Observed Transport and Variability, Frontiers in Marine Science, 6, 260, https://doi.org/10.3389/fmars.2019.00260.

Frierson D., and Coauthors, 2013: Contribution of ocean overturning circulation to tropical rainfall peak in the Northern Hemisphere, Nature Geoscience 6, 940–944, https://doi.org/10.1038/ngeo1987.

Gervais M., Shaman J., and Kushnir Y., 2018: Mechanisms Governing the Development of the North Atlantic Warming Hole in the CESM-LE Future Climate Simulations, J. Climate, 31, 5927–5946, https://doi.org/10.1175/JCLI-D-17-0635.1.

Gervais M., Shaman J., and Kushnir Y., 2019: Impacts of the North Atlantic Warming Hole in Future Climate Projections: Mean Atmospheric Circulation and the North Atlantic Jet, J. Climate, 32, 2673–2689, https://doi.org/10.1175/JCLI-D-18-0647.1.

Goswami B. N., Madhusoodanan M. S., Neema C. P., and Sengupta D., 2006: A physical mechanism for North Atlantic SST influence on the Indian summer monsoon, Geophys. Res. Lett., 33, L02706, https://doi.org/10.1029/2005GL024803.

Gregory J.M., and Coauthors, 2005: A model intercomparison of changes in the Atlantic thermohaline circulation in response to increasing atmospheric CO2 concentration. Geophys. Res. Lett., 32, L12703, https://doi.org/10.1029/2005GL023209.

Hand R., Keenlyside N.S., Omrani N., et al., 2019: The role of local sea surface temperature pattern changes in shaping climate change in the North Atlantic sector, Clim. Dyn., 52, 417–438, https://doi.org/10.1007/s00382-018-4151-1.

Held I. M., and Soden B.J., 2006: Robust Responses of the Hydrological Cycle to Global Warming, J. Climate, 19, 5686–5699, https://doi.org/10.1175/JCLI3990.1.

Henry L., McManus J. F., Curry W. B., Roberts N. L., Piotrowski A. M., and Keigwin L. D., 2016: North Atlantic ocean circulation and abrupt climate change during the last glaciation. Science, 353, 6298, 470–474, https://doi.org/10.1126/science.aaf5529.

Hu S., and Fedorov A. V., 2019: Indian Ocean warming can strengthen the Atlantic meridional overturning circulation, Nature Climate Change, 9, 747-751, https://doi.org/10.1038/s41558-019-0566-x.

Hu, A., L. Van Roekel, W. Weijer, O. A. Garuba, W. Cheng, and B. T. Nadiga, 2020: Role of AMOC in Transient Climate Response to Greenhouse Gas Forcing in Two Coupled Models. *J. Climate*, **33**, 5845–5859, https://doi.org/10.1175/JCLI-D-19-1027.1.

Jackson L. C., Peterson K. A., Roberts C. D., and Wood R. A., 2016: Recent slowing of Atlantic overturning circulation as a recovery from earlier strengthening, Nature Geoscience, 9, 518–522, https://doi.org/10.1038/ngeo2715.

Jackson L.C., Kahana R., Graham T. et al., 2015: Global and European climate impacts of a slowdown of the AMOC in a high resolution GCM, Climate Dynamics, 45, 3299–3316, https://doi.org/10.1007/s00382-015-2540-2.

Keil P., Mauritsen T., Jungclaus J. et al., 2020: Multiple drivers of the North Atlantic warming hole, Nat. Clim. Change, 10, 667–671, https://doi.org/10.1038/s41558-020-0819-8.

Kostov Y., Armour K. C., and Marshall J., 2014: Impact of the Atlantic meridional overturning circulation on ocean heat storage and transient climate change, Geophysical Research Letters, 41, 2108–2116, https://doi.org/10.1002/2013GL058998.

Lenton T. M., Held H., Kriegler E., Hall J.W., Lucht W., Rahmstorf S., and Schellnhuber H.J., 2013: Tipping elements in the Earth's climate system, Proceedings of the National Academy of Sciences of the USA, 105, 1786-1793, https://doi.org/10.1073/pnas.0705414105.

Levang S. J., and Schmitt R.W., 2020: What Causes the AMOC to Weaken in CMIP5?, J. Climate, 33, 1535–1545, https://doi.org/10.1175/JCLI-D-19-0547.1.

Levine A. F. Z., McPhaden M. J., and Frierson D. M. W., 2017: The impact of the AMO on multidecadal ENSO variability, Geophys. Res. Lett., 44, 3877-3886, https://doi.org/10.1002/2017GL072524.

Lin Y.-J., Hwang Y.-T., Ceppi P., and Gregory, J. M., 2019: Uncertainty in the Evolution of Climate Feedback Traced to the Strength of the Atlantic Meridional Overturning Circulation. Geophysical Research Letters, 46, 12,331–12,339, https://doi.org/10.1029/2019GL083084.

Liu, W., Fedorov, A., and Sévellec, F., 2019: The mechanisms of the Atlantic Meridional Overturning Circulation slowdown induced by Arctic sea ice decline, Journal of Climate, 32, 977–996, https://doi.org/10.1029/2019RG000644.

Marshall J., Donohoe A., Ferreira D., and McGee D., 2014: The ocean's role in setting the mean position of the Inter-Tropical Convergence Zone, Climate Dynamics, 42, 1967–1979, https://doi.org/10.1007/s00382-013-1767-z.

Marshall J., Scott J. R., Armour K. C., Campin J. M., Kelley M., and Romanou A., 2015: The ocean's role in the transient response of climate to abrupt greenhouse gas forcing, Climate Dynamics, 44, 2287–2299, https://doi.org/10.1007/s00382-014-2308-0.

McCarthy G., Frajka-Williams E., Johns W. E., Baringer M. O., Meinen C. S., Bryden H. L., Rayner D., Duchez A., Roberts C., and Cunningham S. A., 2012: Observed interannual variability of the Atlantic meridional overturning circulation at 26.5◦N, Geophysical Research Letters, 39, L19 609, https://doi.org/10.1029/2012GL052933.

Menary M.B., and Wood R.A., 2018: An anatomy of the projected North Atlantic warming hole in CMIP5 models, Clim Dyn, 50, 3063–3080, https://doi.org/10.1007/s00382-017-3793-8.

Oudar T., Cattiaux J., and Douville H., 2020: Drivers of the northern extratropical eddy-driven jet change in CMIP5 and CMIP6 models, Geophysical Research Letters, 47, e2019GL086695, https://doi.org/10.1029/2019GL086695.

Rahmstorf S., 2002: Ocean circulation and climate during the past 120,000 years, Nature, 419, 6903, 207–214, https://doi.org/10.1038/nature01090.

Rahmstorf S., Box J. E., Feulner G., Mann. M. E., Robinson A., Rutherford S., and Schaffernicht E.J., 2015: Exceptional twentieth-century slowdown in Atlantic Ocean overturning circulation, Nat. Clim. Change, 5, 5, 475–480, https://doi.org/doi:10.1038/nclimate2554.

Robson J., Hodson D., Hawkins E., and Sutton R., 2013: Atlantic overturning in decline?, Nature Geoscience, 7, 1, 2–3, https://doi.org/10.1038/ngeo2050.

Seager R., Battisti D.S., Yin J., Gordon N., Naik N., Clement A.C., and Cane M.A., 2002: Is the Gulf Stream responsible for Europe's mild winters?, Q.J.R. Meteorol. Soc., 128: 2563-2586, https://doi.org/10.1256/qj.01.128.

Sévellec F., Fedorov A.V., and Liu W., 2017: Arctic sea-ice decline weakens the Atlantic Meridional Overturning Circulation, Nature Climate Change, 7, 604–610, https://doi.org/10.1038/nclimate3353.

Smeed D. A., Josey S. A., Beaulieu C., Johns W. E., Moat B. I., Frajka-Williams E., Rayner D., Meinen C. S., Baringer M. O., Bryden H. L., and McCarthy G. D., 2018: The North Atlantic Ocean Is in a State of Reduced Overturning, Geophysical Research Letters, 45, 1527–1533, https://doi.org/10.1002/2017GL076350.

Smeed D. A., McCarthy G. D., Cunningham S. A., Frajka-Williams E., Rayner D., Johns W. E., Meinen C. S., Baringer M. O., Moat B. I., Duchez A., and Bryden H. L., 2014: Observed decline of the Atlantic meridional overturning circulation 2004–2012, Ocean Science, 10, 29–38, https://doi.org/10.5194/os-10-29-2014.

Sun L., Alexander M., and Deser C., 2018: Evolution of the Global Coupled Climate Response to Arctic Sea Ice Loss during 1990–2090 and Its Contribution to Climate Change, J. Climate, 31, 7823–7843, https://doi.org/10.1175/JCLI-D-18-0134.1.

Talley L. D., 2008: Freshwater transport estimates and the global overturning circulation: Shallow, deep and throughflow components, Progress in Oceanography, 78, 257–303, https://doi.org/10.1016/j.pocean.2008.05.001.

Taylor, K.E., R.J. Stouffer, G.A. Meehl, 2012: An Overview of CMIP5 and the experiment design. Bull. Amer. Meteor. Soc., 93**,** 485-498, https://doi.org/10.1175/BAMS-D-11-00094.1.

Vellinga M., and Wood, R. A., 2008: Impacts of thermohaline circulation shutdown in the twenty-first century, Climatic Change, 91, 1, 43–63. https://doi.org/10.1007/s10584-006-9146-y.

Weijer W., Cheng W., Drijfhout S. S., Federov A.V., Hu A., Jackson L. C., et al., 2019: Stability of the Atlantic Meridional Overturning Circulation: A review and synthesis. Journal of Geophysical Research: Oceans, 124, 5336–5375. https://doi.org/10.1029/2019JC015083.

Weijer W., Cheng W., Garuba O., Hu A., and Nadiga B., 2020: CMIP6 models predict significant 21st century decline of the Atlantic Meridional Overturning Circulation, Geophysical Research Letters, 47, e2019GL086075, https://doi.org/10.1029/2019GL086075.

Winton M., Griffies S. M., Samuels B. L., Sarmiento J. L., and Frölicher T. L., 2013: Connecting Changing Ocean Circulation with Changing Climate, Journal of Climate, 26, 2268–2278, https://doi.org/10.1175/JCLI-D-12-00296.1.

Woollings T., Gregory J., Pinto J., et al., 2012: Response of the North Atlantic storm track to climate change shaped by ocean–atmosphere coupling. Nature Geosci, 5, 313–317, https://doi.org/10.1038/ngeo1438.

Zelinka M. D., Myers T. A., McCoy D. T., Po-Chedley S., Caldwell P. M., Ceppi P., et al., 2020: Causes of higher climate sensitivity in CMIP6 models. Geophysical Research Letters, 47, e2019GL085782, https://doi.org/10.1029/2019GL085782.

Zhang R., Sutton R., Danabasoglu G., Kwon Y.-O., Marsh R., Yeager S. G., et al., 2019: A review of the role of the Atlantic Meridional Overturning Circulation in Atlantic Multidecadal Variability and associated climate impacts. Reviews of Geophysics, 57, 316– 375, https://doi.org/10.1029/2019RG000644.

Zhang, R., and Delworth T.L., 2005: Simulated tropical response to a substantial weakening of the Atlantic thermohaline circulation, J. Climate, 18, 12, 1853–1860, https://doi.org/10.1175/JCLI3460.1.

Zhao J., and Johns W., 2014: Wind-forced interannual variability of the Atlantic Meridional Overturning Circulation at 26.5°N, J. Geophys. Res. Oceans, 119, 2403– 2419, https://doi.org/10.1002/2013JC009407.

Acknowledgements: This project is TiPES contribution ###. We thank Virna Meccia, Paolo Davini, Giuseppe Zappa and Mark Zelinka for helpful discussions. **Funding:** This project has received funding from the European Union's Horizon 2020 research and innovation programme under grant agreement No. 820970 (TiPES). **Author contributions:** All authors conceived the project, J.v.H. and K.B retrieved the data, K.B. analyzed the data and wrote the manuscript. All authors edited the manuscript. **Competing interests:** The authors declare no competing interests. **Data and materials availability:** All model output was obtained through the CMIP5 and CMIP6 public archives and can be accessed at https://esgf-node.llnl.gov/search/cmip5/ and https://esgf-node.llnl.gov/search/cmip6/.

Figures and Tables

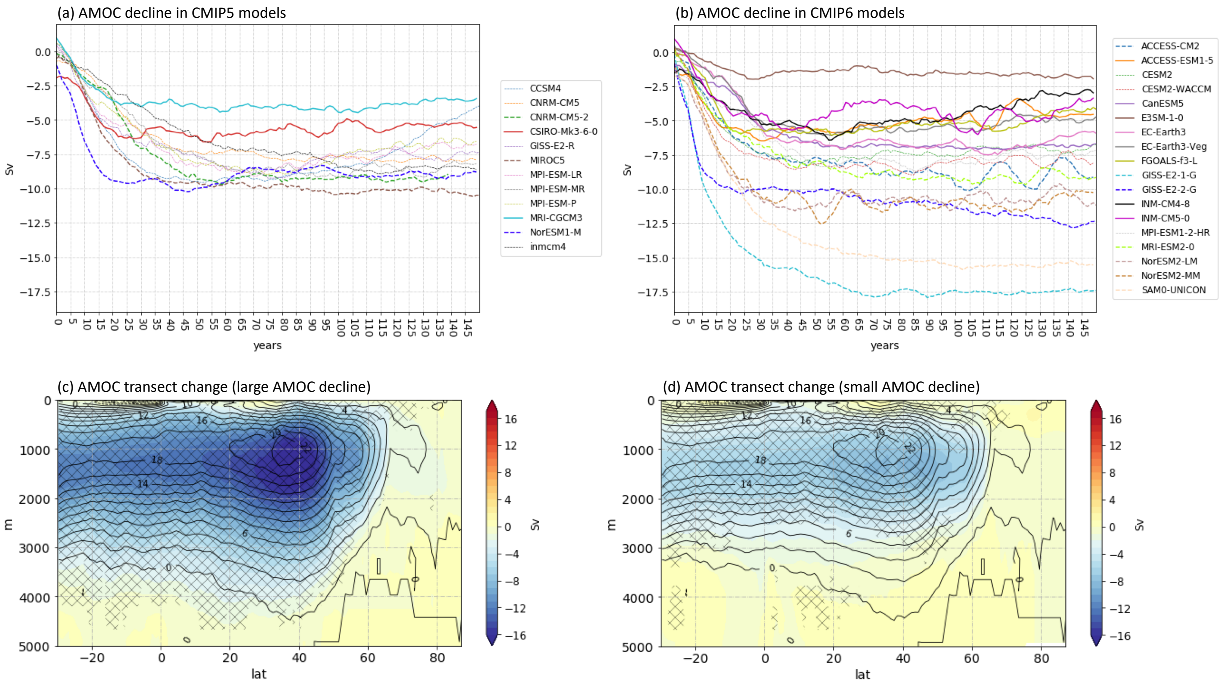

Fig. 1: Inter-model differences in the AMOC response. Panels (a) and (b) show the annual mean AMOC anomalies in the abrupt-4xCO2 simulations at 26.5 °N for (a) CMIP5 and (b) CMIP6 models with respect to the mean AMOC strength computed from the pre-industrial control. A 10-year running average smoothing has been applied to all curves for better visualization. Solid lines represent the models in the small AMOC decline group, while thick dashed lines represent the models in the large AMOC decline group. Models that do not belong to any groups, are represented by thin dashed lines. Panels (c) and (d) show transects of the ocean overturning stream-function in the North Atlantic for (c) the average of the large AMOC decline group, and (d) the average of the small AMOC decline group. Contours show the climatology computed from the pre-industrial control of the (a) 10 large AMOC decline models and (b) 10 small AMOC decline models. The 'x' stippling indicates 'reliability', which is defined where at least 80% of the models in each group agree on the sign of the difference between the model's stream-function change and the median stream-function change of all CMIP5+CMIP6 models.

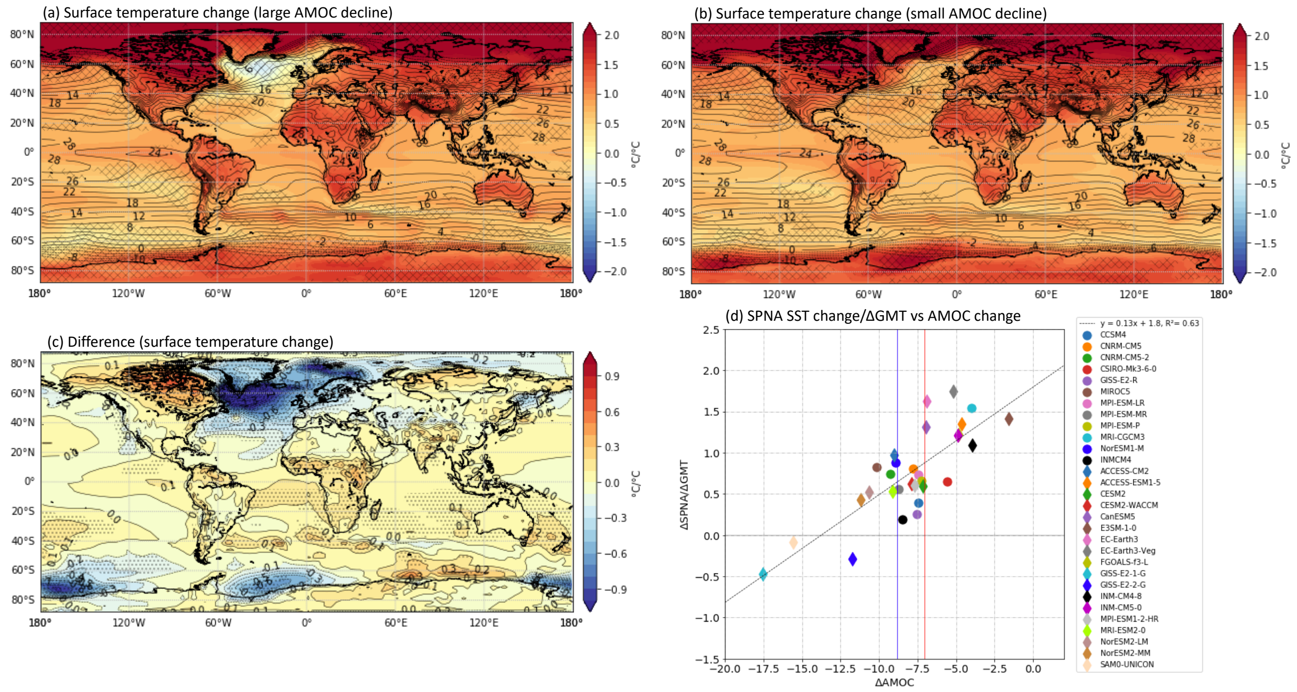

Fig. 2: Surface temperature. Panels (a) and (b) show the annual mean surface temperature change of the abrupt-4xCO2 minus pre-industrial control for (a) the average of the large AMOC decline group and (b) the average of the AMOC decline group. Panel (c) is their difference (a minus b). Each model is divided by its respective ΔGMT, hence the units are °C per degree of global warming. In panels (a) and (b) the 'x' stippling indicates 'reliability' and is defined where at least 60% of the models in each group agree on the sign of the difference between the model's surface temperature change and the median surface temperature change of all CMIP5+CMIP6 models. In panel (c) the '*' stippling indicates statistical significance, which is defined where the Student's t-test is significant at the 90% level. In panels (a), (b) and (c), contours show the climatological mean precipitation computed from all CMIP5+CMIP6 models. Panel (d) shows the change in sup-polar North Atlantic SST change (ΔSPNA) divided by ΔGMT against AMOC change (ΔAMOC) in units of Sv. Circles represent CMIP5 models, while diamonds represent CMIP6 models. The black line is the linear regression. The Pearson's r correlation coefficient is 0.8. The blue and red vertical lines represent the lower and upper terciles of the ΔAMOC distribution. Models to the left of the blue line belong to the large AMOC decline group, while models to the right of the red line belong to the small AMOC decline group.

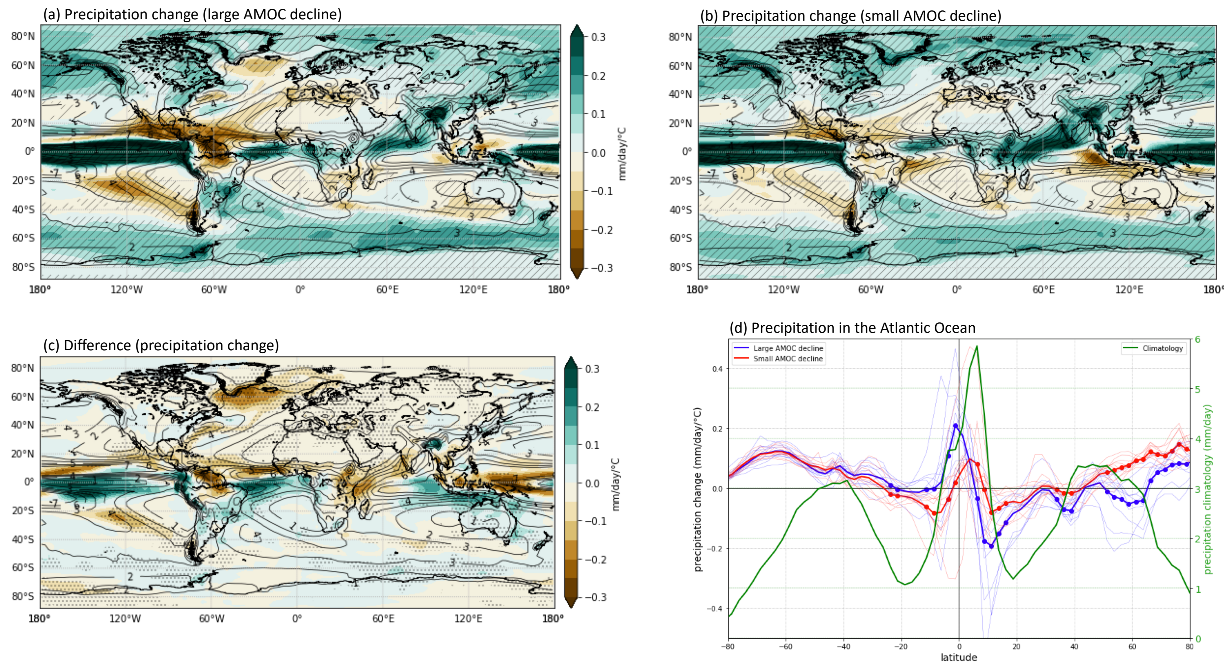

Fig. 3: Precipitation. Panels (a) and (b) show the annual mean precipitation change of the abrupt-4xCO2 minus the pre-industrial control for (a) the average of the large AMOC decline group and (b) the average of the AMOC decline group. Panel (c) is their difference (a minus b). Each model is divided by its respective ΔGMT, hence the units are mm/day per degree of global warming. In panels (a) and (b) the '/' stippling indicates 'reliability', and is defined where at least 80% of the models in each group agree on the sign of the change from the pre-industrial control climatology. In panel (c) the '*' stippling indicates statistical significance, which is defined where the Student's t-test is significant at the 90% level. In panels (a), (b) and (c), contours show the climatological mean precipitation computed from all CMIP5+CMIP6 models. Panel (d) shows the zonal mean precipitation change in the North Atlantic sector in the (blue) large AMOC decline group and (red) small AMOC decline group. Thick lines are the group averages, while thin lines show each group member. Round markers indicate where the Student's t-test between the means of the two groups is significant at the 90% level. The green line is the zonal mean precipitation climatology computed from the pre-industrial control of all CMIP5+CMIP6 models. Units are of mm/day and the corresponding scale is located on right-side y-axis.

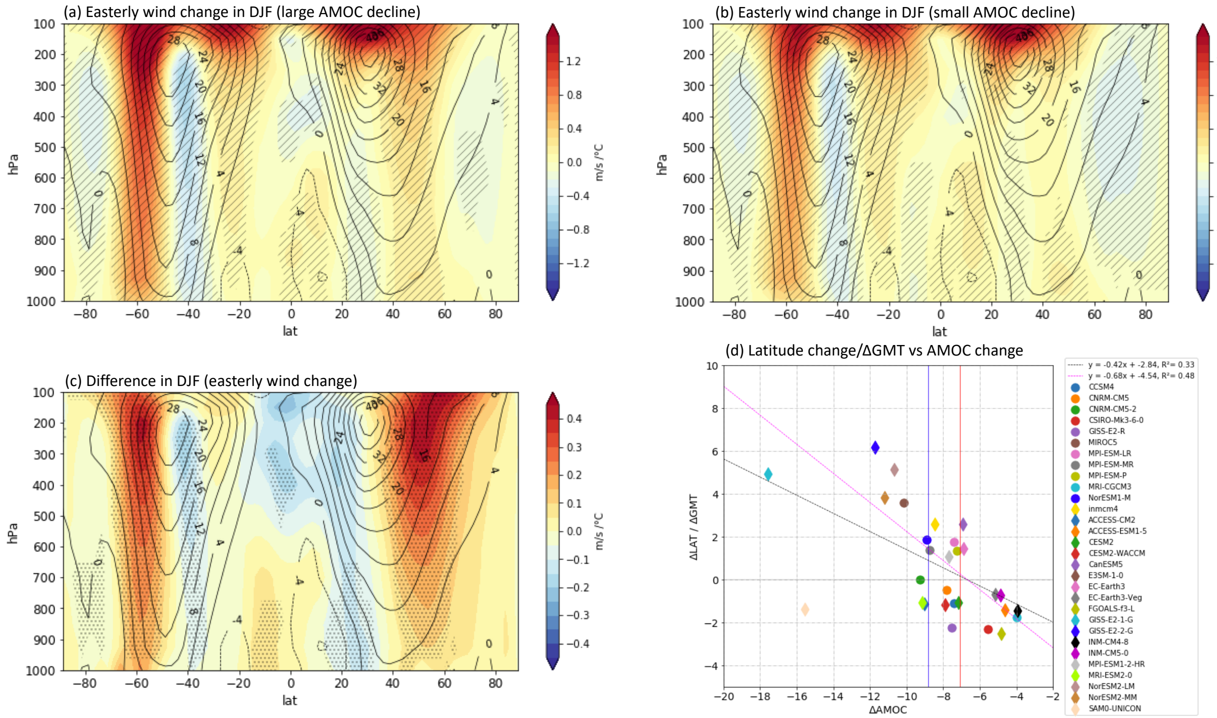

Fig. 4: Easterly wind speed in DJF. Panels (a) and (b) show the zonal mean easterly wind speed change in DJF of the abrupt-4xCO2 minus the pre-industrial control for (a) the average of the large AMOC decline group and (b) the average of the AMOC decline group. Panel (c) is their difference (a minus b). Each model is divided by its respective ΔGMT, hence the units are m/s per degree of global warming. In panels (a) and (b) the '/' stippling indicates 'reliability', and is defined where at least 80% of the models in each group agree on the sign of the change from the pre-industrial control climatology. In panel (c) the '*' stippling indicates statistical significance, which is defined where the Student's t-test is significant at the 90% level. In panels (a), (b) and (c), contours show the climatological zonal mean easterly wind speed in DJF computed from all CMIP5+CMIP6 models. Panel (d) shows the change in the latitude of the maximum wind speed at 250hPa (ΔLAT) divided by ΔGMT against AMOC change (ΔAMOC). Circles represent CMIP5 models, while diamonds represent CMIP6 models. The dashed black line is the linear regression including all models, while the dashed magenta line is the linear regression excluding the two outliers (GISS-E2-1-G and SAM0-UNICON). . The Pearson's r correlation coefficient is -0.58 for all models, and -0.7 excluding the two outliers. The blue and red vertical lines represent the lower and upper terciles of the ΔAMOC distribution. Models to the left of the blue line belong to the large AMOC decline group, while models to the right of the red line belong to the small AMOC decline group.

Table 1: Mean values in the large and small AMOC groups. The differences between the means are statistically significant at the 90% level of a two-side Student's t-test except the values in *italics*.

	Mean	
	Large ΔAMOC	Small ΔAMOC
Mean AMOC strength (pre-industrial control)	21.46 Sv	16.82 Sv
Mean AMOC strength 4xCO2 (years 90-139)	*10.13 Sv*	*11.98 Sv*
AMOC change	-11.32 Sv	-4.84 Sv
Percent AMOC change	-53.89 %	-29.33 %
SPNA SST change	1.99 °C	7.68 °C
GMT change	4.53 °C	5.67 °C
SPNA/GMT change	0.41	1.32

Supplementary Materials

Figures

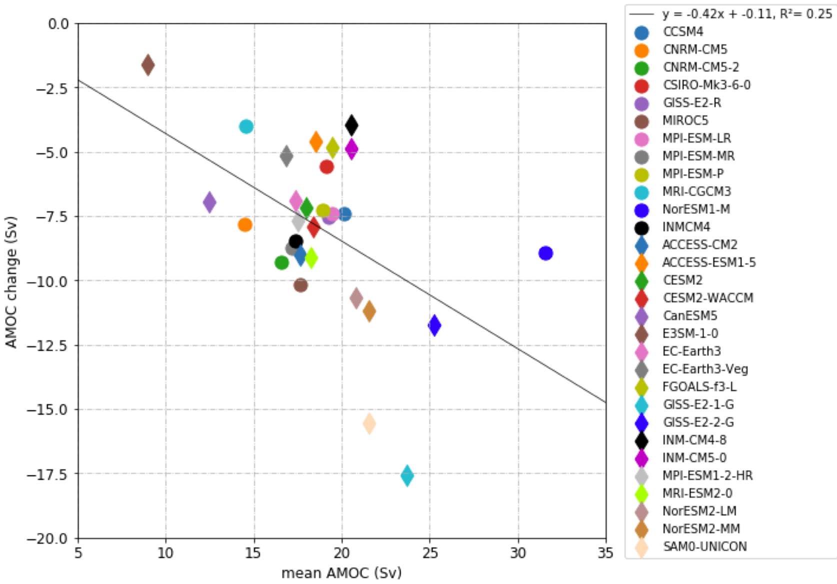

Fig. S1: Dependence of AMOC change on the mean AMOC strength. Scatterplot of change in AMOC (abrupt-4xCO2 minus pre-industrial control) against mean AMOC (pre-industrial control) for all models. Circles represent CMIP5 models, while diamonds represent CMIP6 models. The black line is the least-square regression of AMOC change on mean AMOC. The Pearson's r correlation coefficient is -0.50.

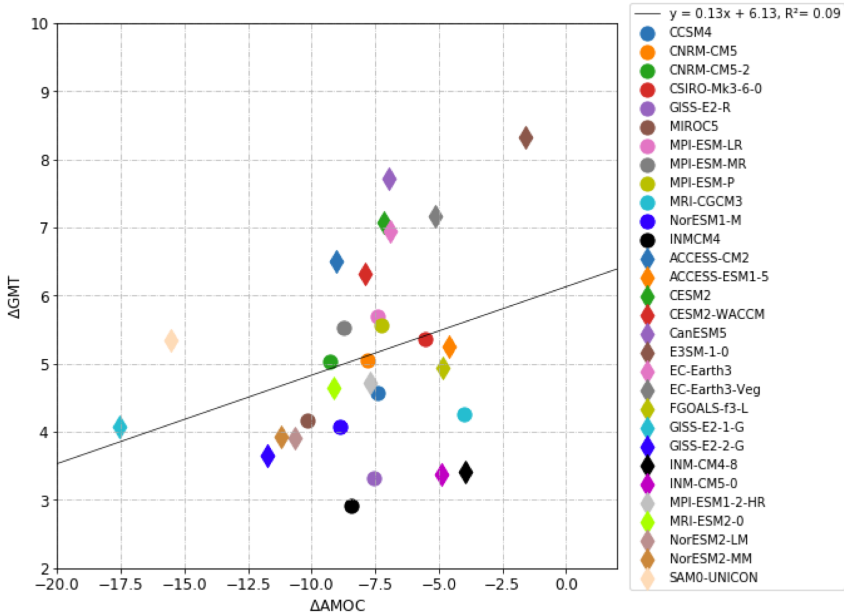

Fig. S2: Dependence of global mean temperature change on AMOC change. Scatterplot of change in Global Mean Temperature (ΔGMT) (abrupt-4xCO2 minus pre-industrial control) against change in AMOC (abrupt-4xCO2 minus pre-industrial control) for all models. Circles represent CMIP5 models, while diamonds represent CMIP6 models. The black line is the least-square regression of ΔGMT on ΔAMOC. The Pearson's r correlation coefficient is 0.31.

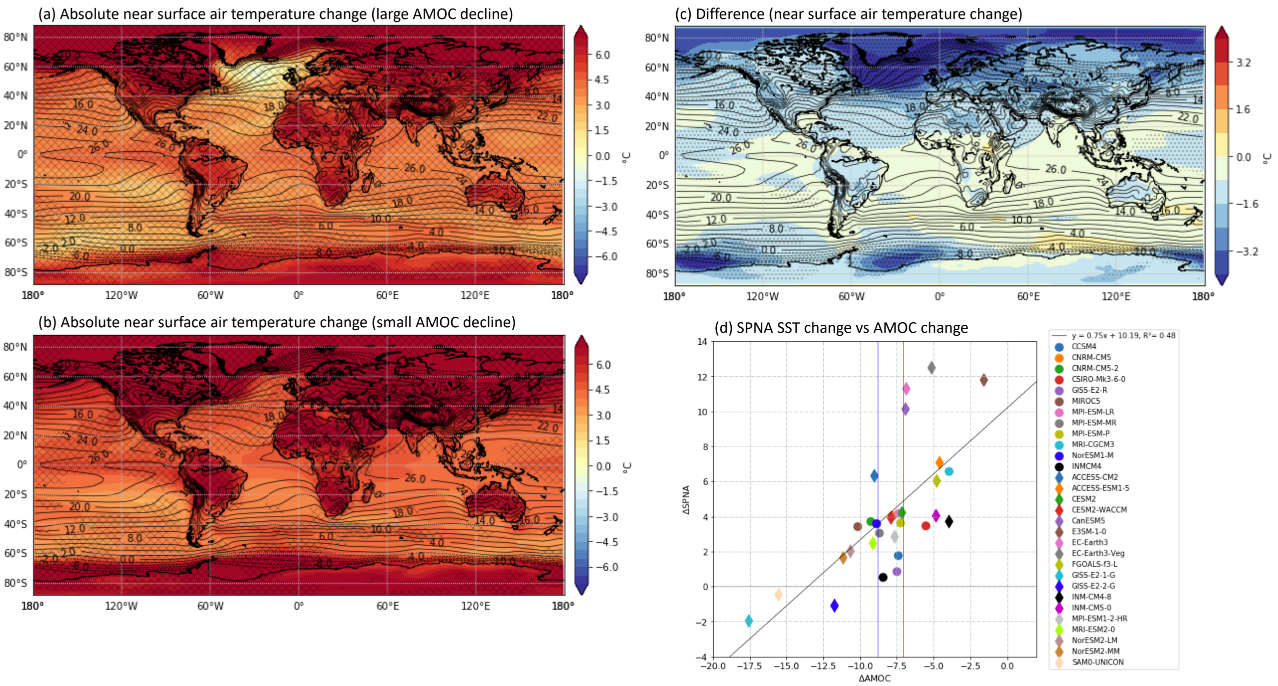

Fig. S3: Near surface air temperature. Panels (a) and (b) show the annual mean near surface air temperature change of the abrupt-4xCO2 minus pre-industrial control for (a) the average of the large AMOC decline group and (b) the average of the AMOC decline group. Panel (c) is their difference (a minus b). Units are °C. In panels (a) and (b) the 'x' stippling indicates 'reliability' and is defined where at least 60% of the models in each group agree on the sign of the difference between the model's near surface air temperature change and the median near surface air temperature change of all CMIP5+CMIP6 models. In panel (c) the '*' stippling indicates statistical significance, which is defined where the Student's t-test is significant at the 90% level. In panels (a), (b) and (c), contours show the climatological mean near surface air temperature computed from all CMIP5+CMIP6 models. Panel (d) shows the change in sup-polar North Atlantic SST change (ΔSPNA) in units of °C against AMOC change (ΔAMOC) in units of Sv. Circles represent CMIP5 models, while diamonds represent CMIP6 models. The black line is the linear regression. The Pearson's r correlation coefficient is 0.69. The blue and red vertical lines represent the lower and upper terciles of the ΔAMOC distribution. Models to the left of the blue line belong to the large AMOC decline group, while models to the right of the red line belong to the small AMOC decline group.

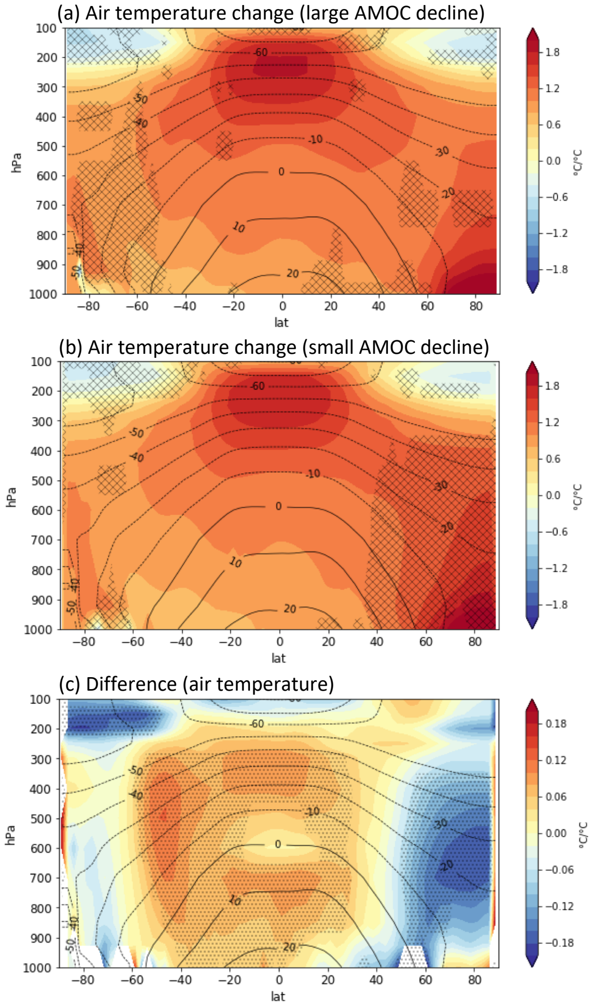

Fig. S4: Zonal mean air temperature. Panels (a) and (b) show the zonal mean air temperature change of the abrupt-4xCO2 from the pre-industrial control for (a) the average of the large AMOC decline group and (b) the average of the AMOC decline group. Panel (c) is their difference (a minus b). Each model is divided by their respective ΔGMT, hence the units are °C per degree of global warming, In panels (a) and (b) the ‘x’ stippling indicates ‘reliability’ and is defined as where at least 60% of the models in each group agree on the sign of the difference between the model’s surface air temperature change and the median air temperature change of all CMIP5+CMIP6 models. In panel (c) the ‘*’ stippling indicates statistical significance, which is defined where the Student’s t-test is significant at the 80% level. In panels (a), (b) and (c), contours show the climatological zonal mean air temperature.

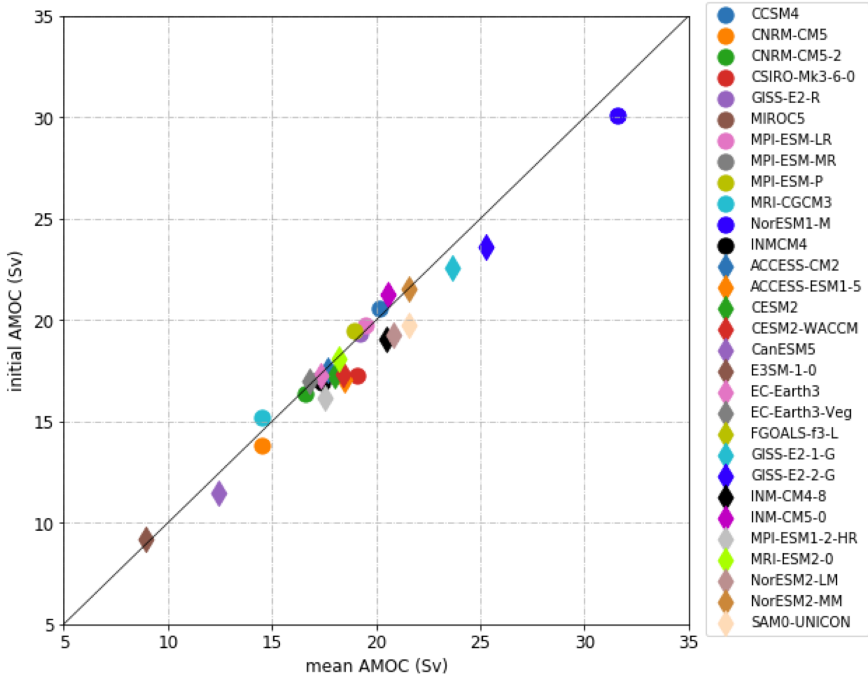

Fig. S5: Estimates of mean AMOC strength. Scatterplot of the annual mean AMOC in the first year of the abrupt-4xCO2 (‘initial AMOC’) against mean AMOC computed from the pre-industrial control (‘mean AMOC’). Circles represent CMIP5 models, while diamonds represent CMIP6 models. In back, the 1:1 line.

Tables

	Model	Archive	Mean AMOC strength [Sv]	Mean AMOC strength 4xCO2 [Sv]	AMOC change [Sv]	AMOC change [%]	Sub-Polar North Atlantic (SPNA) SST change [°C]	Global mean near-surface air Temperature (GMT) change [°C]	SPNA SST/GMT change
1	CCSM4	CMIP5	20.14	12.72	-7.42	-37%	1.79	4.57	0.39
2	CNRM-CM5	CMIP5	14.51	6.71	-7.80	-54%	4.06	5.05	0.80
3	CNRM-CM5-2	CMIP5	16.60	7.33	-9.27	-56%	3.73	5.03	0.74
4	CSIRO-Mk3-6-0	CMIP5	19.10	13.55	-5.55	-29%	3.47	5.36	0.65
5	GISS-E2-R	CMIP5	19.24	11.70	-7.54	-39%	0.86	3.33	0.26
6	MIROC5	CMIP5	17.67	7.50	-10.17	-58%	3.46	4.17	0.83
7	MPI-ESM-LR	CMIP5	19.48	12.06	-7.42	-38%	4.17	5.70	0.73
8	MPI-ESM-MR	CMIP5	17.19	8.46	-8.73	-51%	3.06	5.52	0.55
9	MPI-ESM-P	CMIP5	18.95	11.69	-7.26	-38%	3.66	5.57	0.66
10	MRI-CGCM3	CMIP5	14.52	10.53	-3.99	-27%	6.58	4.26	1.55
11	NorESM1-M	CMIP5	31.57	22.66	-8.91	-28%	3.60	4.07	0.88
12	inmcm4	CMIP5	17.38	8.93	-8.46	-49%	0.56	2.92	0.19
13	ACCESS-CM2	CMIP6	17.64	8.61	-9.03	-51%	6.34	6.50	0.98
14	ACCESS-ESM1-5	CMIP6	18.49	13.88	-4.61	-25%	7.09	5.25	1.35
15	CESM2	CMIP6	18.01	10.84	-7.17	-40%	4.23	7.07	0.60
16	CESM2-WACCM	CMIP6	18.39	10.49	-7.90	-43%	3.95	6.32	0.63
17	CanESM5	CMIP6	12.44	5.50	-6.94	-56%	10.16	7.71	1.32
18	E3SM-1-0	CMIP6	8.95	7.35	-1.59	-18%	11.79	8.32	1.42
19	EC-Earth3	CMIP6	17.37	10.48	-6.89	-40%	11.29	6.94	1.63
20	EC-Earth3-Veg	CMIP6	16.82	11.66	-5.16	-31%	12.50	7.17	1.74
21	FGOALS-f3-L	CMIP6	19.48	14.65	-4.83	-25%	6.05	4.95	1.22
22	GISS-E2-1-G	CMIP6	23.67	6.10	-17.57	-74%	-1.93	4.07	-0.47
23	GISS-E2-2-G	CMIP6	25.26	13.52	-11.75	-46%	-1.05	3.65	-0.29
24	INM-CM4-8	CMIP6	20.51	16.55	-3.96	-19%	3.75	3.42	1.09
25	INM-CM5-0	CMIP6	20.55	15.67	-4.88	-24%	4.08	3.37	1.21
26	MPI-ESM1-2-HR	CMIP6	17.51	9.83	-7.69	-44%	2.88	4.73	0.61
27	MRI-ESM2-0	CMIP6	18.22	9.09	-9.13	-50%	2.47	4.64	0.53
28	NorESM2-LM	CMIP6	20.82	10.16	-10.66	-51%	2.04	3.90	0.52
29	NorESM2-MM	CMIP6	21.57	10.38	-11.19	-52%	1.68	3.93	0.43
30	SAM0-UNICON	CMIP6	21.55	5.99	-15.56	-72%	-0.44	5.35	-0.08
		Min	**8.95 Sv**	**5.50 Sv**	**-1.59 Sv**	**-18%**	**-1.93 °C**	**2.92 °C**	**-0.47**
		Max	**31.57 Sv**	**22.66 Sv**	**-17.57 Sv**	**-74%**	**12.50 °C**	**8.32 °C**	**1.74**

Table S1: List of CMIP5 and CMIP6 models. Note that for the FGOALS-f3-L model we could not retrieve the ocean meridional stream-function from the pre-industrial control simulation, hence we used the mean of the first year of the abrupt-4xCO2 simulation to compute the mean AMOC strength.

	Model	Archive	Mean AMOC strength [Sv]	AMOC strength 4xCO2 [Sv]	AMOC change [Sv]	AMOC change [%]	Sub-Polar North Atlantic (SPNA) SST change [°C]	Global mean near-surface air Temperature (GMT) change [°C]	SPNA SST/GMT change
1	CSIRO-Mk3-6-0	CMIP5	19.10	13.55	-5.55	-29%	3.47	5.36	0.65
2	MRI-CGCM3	CMIP5	14.52	10.53	-3.99	-27%	6.58	4.26	1.55
3	ACCESS-ESM1-5	CMIP6	18.49	13.88	-4.61	-25%	7.09	5.25	1.35
4	CanESM5	CMIP6	12.44	5.50	-6.94	-56%	10.16	7.71	1.32
5	E3SM-1-0	CMIP6	8.95	7.35	-1.59	-18%	11.79	8.32	1.42
6	EC-Earth3	CMIP6	17.37	10.48	-6.89	-40%	11.29	6.94	1.63
7	EC-Earth3-Veg	CMIP6	16.82	11.66	-5.16	-31%	12.50	7.17	1.74
8	FGOALS-f3-L	CMIP6	19.48	14.65	-4.83	-25%	6.05	4.95	1.22
9	INM-CM4-8	CMIP6	20.51	16.55	-3.96	-19%	3.75	3.42	1.09
10	INM-CM5-0	CMIP6	20.55	15.67	-4.88	-24%	4.08	3.37	1.21
		Mean	**16.82 Sv**	**11.98 Sv**	**-4.84 Sv**	**-29%**	**7.68 °C**	**5.67 °C**	**1.32**
1	CNRM-CM5-2	CMIP5	16.60	7.33	-9.27	-56%	3.73	5.03	0.74
2	MIROC5	CMIP5	17.67	7.50	-10.17	-58%	3.46	4.17	0.83
3	NorESM1-M	CMIP5	31.57	22.66	-8.91	-28%	3.60	4.07	0.88
4	ACCESS-CM2	CMIP6	17.64	8.61	-9.03	-51%	6.34	6.50	0.98
5	GISS-E2-1-G	CMIP6	23.67	6.10	-17.57	-74%	-1.93	4.07	-0.47
6	GISS-E2-2-G	CMIP6	25.26	13.52	-11.75	-46%	-1.05	3.65	-0.29
7	MRI-ESM2-0	CMIP6	18.22	9.09	-9.13	-50%	2.47	4.64	0.53
8	NorESM2-LM	CMIP6	20.82	10.16	-10.66	-51%	2.04	3.90	0.52
9	NorESM2-MM	CMIP6	21.57	10.38	-11.19	-52%	1.68	3.93	0.43
10	SAM0-UNICON	CMIP6	21.55	5.99	-15.56	-72%	-0.44	5.35	-0.08
		Mean	**21. 45 Sv**	**10.13 Sv**	**-11.32 Sv**	**-54%**	**1.99 °C**	**4.53 °C**	**0.41**

Table S2: Large and Small AMOC decline groups. Top: list of models belonging to the small AMOC decline group (red); Bottom: list of the models belonging to the large AMOC decline group (blue).